coatings

Article

Coupled Modeling of Anisotropic Stress-Induced Diffusion and Trapping of Nitrogen in Austenitic Stainless Steel during Nitriding and Thermal Annealing

Teresa Moskaliovienė [1], Paulius Andriūnas [1] and Arvaidas Galdikas [1,2,*]

[1] Physics Department, Kaunas University of Technology, Studentu 50, LT-51368 Kaunas, Lithuania
[2] Department of Physics, Mathematics and Biophysics, Lithuanian University of Health Sciences, Eivenių Str. 4, LT-50166 Kaunas, Lithuania
* Correspondence: arvaidas.galdikas@ktu.lt; Tel.: +370-600-48-897

Abstract: In this paper, nitrogen diffusion is investigated in single-crystalline austenitic stainless steel during modified layer formation and thermal annealing. A generalized system of diffusion equations is derived within a thermodynamic framework from Fick's laws, which describe nitrogen flux under multiple driving forces, including a concentration gradient and the gradient of hydrostatic stress. Trapping and detrapping phenomena are considered within this model, and nitrogen flux is distinguished depending on whether nitrogen is in a lattice or a trapping site. Furthermore, the effects of anisotropic elasticity in single-crystal austenitic stainless steel on the stress field are investigated. The proposed model is used to simulate the nitrogen transportation process in single-crystalline AISI 316L during ion beam nitriding and after isothermal annealing at three different crystalline orientations. The results of our theoretical predictions are compared with experimental results taken from the literature. It is shown that during isothermal annealing, nitrogen diffusion becomes significantly slower than during nitriding. The diffusion coefficient during the annealing process, compared with the nitriding process, decreases by factors of 4.3, 3.3, and 2.5 for the orientations (001), (011), and (111), respectively.

Keywords: nitriding; thermal annealing; stress-induced diffusion; trapping; austenitic stainless steel; kinetic model

check for updates

Citation: Moskaliovienė, T.; Andriūnas, P.; Galdikas, A. Coupled Modeling of Anisotropic Stress-Induced Diffusion and Trapping of Nitrogen in Austenitic Stainless Steel during Nitriding and Thermal Annealing. *Coatings* **2023**, *13*, 415. https://doi.org/10.3390/coatings13020415

Academic Editors: Torsten Brezesinski and Ben Breitung

Received: 21 December 2022
Revised: 26 January 2023
Accepted: 10 February 2023
Published: 12 February 2023

Copyright: © 2023 by the authors. Licensee MDPI, Basel, Switzerland. This article is an open access article distributed under the terms and conditions of the Creative Commons Attribution (CC BY) license (https://creativecommons.org/licenses/by/4.0/).

1. Introduction

Austenitic stainless steels (ASSs) are attractive materials for many industrial applications due to their excellent corrosion resistance. Even so, their low hardness level and poor tribological properties, such as wear resistance, limit their widespread application. One of the most promising surface hardening methods is low-temperature nitriding. This thermo-chemical surface treatment has been shown to improve the surface hardness, friction resistance, and tribological properties of ASSs [1–11]. The origin of these improvements is that the nitrogen diffusion process results in the formation of an expanded austenite (called the γ_N phase) layer [4,9,12,13], which essentially is a supersaturated solid solution of interstitial nitrogen atoms (with nitrogen content of up to 40 at.%) in austenite (γ phase) and without chromium nitride precipitation. The γ_N phase shows very high hardness (up to 1500 HV) and is wear- and corrosion-resistant. Various nitriding technologies have been used so far to obtain layers composed of the γ_N phase. The most typical methods include gas and plasma processes. It has been shown that it is also possible to obtain γ_N phase coatings via reactive magnetron sputtering of stainless steel with the addition of nitrogen to the sputtering gas [14–20]. It was confirmed that γ_N phase coatings obtained via magnetron sputtering show good adhesion [18], and their properties and structure are similar to the the γ_N phase produced via gas or plasma nitriding.

The main limitation of γ_N phase material is its metastability. Many studies [21–27], by means of isothermal annealing and in situ TEM heating observations, have shown that even at 450 °C, the γ_N phase decomposes and chromium or iron nitrides can precipitate, which negatively affects the corrosion resistance of the steel. For this reason, nitriding processes are conducted at temperatures below 450 °C. It was also observed that not only is temperature highly important for the formation of nitrides, but so is treatment duration. Moreover, an increase in nitrogen in the treatment atmosphere leads to the formation of a γ_N phase with a higher nitrogen content and accelerates the formation of nitrides in the layer [27]. Despite the fact that considerable experimental investigations have been performed on the thermal stability of the γ_N phase, there are no theoretical models that describe and simulate the processes during annealing.

The next important aspect is related to the fact that nitrogen supersaturation accompanies γ-lattice expansion and that the crystalline structure of the γ_N phase is essentially different from that of the original ASS matrix [4,5,7,8,28–32]. The most important experimental evidence leading to the discovery of the γ_N phase came from the exhaustive XRD phase identification works in Refs. [4,29–31,33], where the γ_N phase peaks apparently look similar to those from the austenite substrate, but all of them are shifted to lower angles and appear to be broader compared to those from the austenite substrate. Further, the $\gamma_N(200)$ positions are more deviated relative to the $\gamma(200)$ diffraction angle than the other planes, demonstrating that the expansion, and thus, the level of nitrogen supersaturation are strongly dependent on the crystallographic orientation [4,30–33]. This effect of anisotropic lattice expansion could be explained by the residual compressive stress developed during nitriding, which varies as a function of crystallographic orientation of the ASS specimen due to the elastically anisotropic nature of austenite [33–37]. The supersaturation of the interstitials causes larger lattice expansion, but the untreated core will constrain the expansion, thus forming very high residual stress in the γ_N phase. During the diffusion of nitrogen atoms in the steel matrix, the gradient of chemical potential serves as the driving force, and the interstitial nitrogen atoms diffuse from high to low chemical potential. Moreover, when the interstitial nitrogen atom occupies the site, the induced compressive stress increases the chemical potential. Accordingly, the chemical potential gradient increases and, thus, diffusion may be enhanced, as was shown in our previous studies [35,38].

Several theoretical models of rapid interstitial diffusion in expanded austenite have been proposed in recent decades, and each of them highlights some particular features. The models are mainly divide into three groups: (1) the models that consider the influence of hydrostatic stress on nitrogen diffusion [35,38–43]; (2) the models that account for diffusion and trapping/detrapping mechanisms [44–46]; and (3) the models based on concentration-dependent diffusion concepts [47]. In general, the trapping/detrapping and stress–diffusivity coupling concepts could provide insights into the phenomenon of high diffusivity of interstitials in expanded austenite. According to the trapping/detrapping model, nitrogen is trapped at chromium sites (trap sites), resulting in the generation of a highly nitrogen-enriched austenite phase layer [44–46]. Once all trap sites are occupied, any additional incoming nitrogen can diffuse rapidly through the austenite layer, i.e., the system contains two types of interstitial atom subjected to different interactions with the lattice and, hence, that have different diffusivities. The next important aspect is related to the fact that the nitrogen diffusion process is driven by the concentration gradient of nitrogen atoms and by migration due to lowering of the chemical potential, induced by hydrostatic stress. All of these mechanisms are very important for accurate modeling of the nitrogen transport process in expanded austenite.

Against the above background, the main aim of the present work is to simulate the fully coupled stress-diffusion and trapping/detrapping processes of nitrogen in expanded austenite during modified layer formation and thermal annealing. With this objective, a generalized system of diffusion equations is derived within a thermodynamic framework from Fick's laws, which describe nitrogen flux under multiple driving forces, including a concentration gradient and the gradient of hydrostatic stress. Trapping and detrapping

phenomena are considered within this model, and nitrogen flux is distinguished depending on whether nitrogen is in a lattice or a trapping site. Furthermore, the effects of anisotropic elasticity in single-crystal ASS on the stress field are involved. The proposed model was used to simulate the nitrogen transportation process in single-crystalline AISI 316L during ion beam nitriding and after isothermal annealing at three different crystalline orientations ((100), (110), and (111)). The results of the simulations are discussed and validated on the basis of experimental measurements from the literature.

2. The Governing Equations of the Nitrogen Transport Model

A kinetic model for nitrogen diffusion in ASS that takes into account stress-induced diffusion and the trapping/detrapping mechanism is proposed in our work [46]. To incorporate the effect of traps into the nitrogen transport equation, we follow the equilibrium theory presented by Oriani [48] to consider a lattice consisting of two kinds of site for occupancy by nitrogen. The model hence distinguishes between free lattice nitrogen (diffusive; N_D) and trapped nitrogen (trapped; N_T). Further, the relevance of stress in nitrogen transport in ASS is well known and described in our previous works [35,38–40]. According to the stress-assisted diffusion model, the driving force for diffusion is the gradient of chemical potential, which is a function of nitrogen concentration and hydrostatic stress. So, considering the effect of hydrostatic stress on the chemical potential of nitrogen at the lattice sites, the nitrogen diffusion process can be expressed as follows [35,38–40,46,49]:

$$\frac{\partial N}{\partial t} = \frac{\partial N_D}{\partial t} + \frac{\partial N_T}{\partial t} = \nabla(D\nabla N_D) + \nabla\left(\frac{D \cdot V_N \cdot N_D}{RT}\nabla\sigma\right) \quad (1)$$

where N_D and N_T are the nitrogen concentrations at the lattice and trapping sites; D is the diffusion coefficient of interstitial nitrogen atoms in a stress-free ASS matrix; σ is the hydrostatic stress; V_N is the partial molar volume of interstitial in the ASS matrix; and R and T are the ideal gas constant and the absolute temperature, respectively.

However, there are two unknowns (concentration N_D and N_T), and both variables should be connected using kinetic or thermodynamic assumptions. According to Oriani [48], when the trapping process is assumed to be instantaneous, the nitrogen concentration in the lattice is assumed to be in equilibrium with the concentration in the traps. So, if the equilibrium between the traps and interstitial sites is considered, the concentration in the traps can be expressed as [44,46,48–50]:

$$\frac{\partial N_T}{\partial t} = K \cdot \left[N_D(H_t - N_T) - N_0 \cdot N_T \cdot e^{\left(\frac{-E_B}{k_B T}\right)}\right] \quad (2)$$

where $K = 4\pi R_t \cdot D$; $D = D_0 e^{-E_A/k_B T}$; H_t is the concentration of the traps; E_B is the detrapping activation energy; E_A is the diffusion activation energy; D_0 is the pre-exponential factor of diffusion; N_0 is the concentration of host atoms; R_t is a characteristic capture radius of an individual trap site taken as the lattice constant; and k_B is the Boltzmann constant. This trap model is based on several assumptions, i.e., it was assumed that (1) traps are isolated and that transport between traps occurs via lattice diffusion; (2) only one type of trap site (which is associated with Cr atoms) is considered; and (3) the concentration of traps is constant and each trap site is allowed to bind only one nitrogen atom.

In general, to solve Equations (1) and (2), a fully coupled analysis is required to understand the dependence of stress state on nitrogen diffusion and vice versa. So, in order to evaluate the compressive stress and the compositional strain induced by interstitial nitrogen atom diffusion in expanded austenite, a mechanical model recently proposed in our previous work [35,38] was used:

$$\sigma(hkl) = \frac{1}{(S_{11} - P_{hkl} \cdot S_{44}(Z-1))} \cdot \frac{\beta_N}{a_0} \cdot N = -X_{stress(hkl)} \cdot N \quad (3)$$

where σ(*hkl*) is compositionally induced biaxial compressive residual stress in the [*h k l*] direction; *N* is the mean concentration of nitrogen interstitials; $X_{stress(hkl)}$ is the anisotropic proportionality constant in any crystallographic direction [*h k l*] (or anisotropic stress factor), which depends on the so-called orientation factor $P_{hkl} = \left(h^2 \cdot k^2 + h^2 \cdot l^2 + k^2 \cdot l^2\right) \cdot \left(h^2 + k^2 + l^2\right)^{-2}$ [51] and on the Young's modulus $E_{hkl} = (S_{11} - 2 \cdot P_{hkl} \cdot (S_{11} - S_{12} - \frac{1}{2}S_{44}))^{-1} = (S_{11} - P_{hkl} \cdot S_{44}(Z-1))^{-1}$, where *h*, *k*, and *l* are the Miller indexes, and S_{11}, S_{12}, and S_{44} are independent intrinsic single-crystal elastic constants (elastic compliances) and the Zener ratio [52] $Z = \frac{2(S_{11}-S_{12})}{S_{44}}$. In addition, a linear relationship exists between the total strain in the [*h k l*] direction. The generalized Hooke's law was used to express the relationship between stress and strain, i.e., $\varepsilon(hkl) = \frac{1}{E_{hkl}} \cdot \sigma(hkl)$), and the mean concentration of interstitials in the expanded austenite, i.e., $\varepsilon(hkl) = \frac{\beta_N}{a_0} \cdot N$ [38], where β_N is Vegard's constant for interstitial nitrogen atoms dissolved in austenite and a_0 is the lattice parameter of the austenite (strain-free).

Finally, based on mass conservation, with the diffusion-induced anisotropic stress and stress–diffusivity coupling given above, we can now develop the generalized set of model equations (by assuming only one type of trap and unidirectional diffusion along the *x* direction):

$$\frac{\partial N_D}{\partial t} = \Phi_{0(hkl)} + \frac{\partial}{\partial x}\left(D\frac{\partial N_D}{\partial x}\right) - \frac{\partial}{\partial x}\left(\frac{D \cdot V_N \cdot N_D \cdot X_{stress(hkl)}}{RT}\frac{\partial N}{\partial x}\right) - v_{sp}\frac{\partial N_D}{\partial x} - \frac{\partial N_T}{\partial t} \quad (4)$$

$$\frac{\partial N_T}{\partial t} = K \cdot \left[N_D(H_t - N_T) - N_0 \cdot N_T \cdot e^{\left(\frac{-E_B}{k_B T}\right)}\right] - v_{sp}\frac{\partial N_T}{\partial x} \quad (5)$$

$$\frac{\partial N}{\partial t} = \frac{\partial N_D}{\partial t} + \frac{\partial N_T}{\partial t} \quad (6)$$

where $\Phi_{0(hkl)}$ is the anisotropic adsorption term, which describes the process of interstitial nitrogen atom adsorption on the ASS surface (i.e., for *x* = 0): $\Phi_{0(hkl)} = i_N \cdot \alpha_{N(hkl)} \cdot (N_0 - N_D(0,t) - N_T(0,t))$, where i_N is the relative flux of incident nitrogen atoms to the surface, and $\alpha_{N(hkl)} = \alpha_N \cdot \left(h^2 + k^2 + l^2\right)^{-1/2}$ is the nitrogen adsorption probability, which depends on the crystal orientation [35,38]. Moreover, the model takes into account the erosion effect at the steel surface due to nitrogen ion irradiation, where v_{sp} is the velocity of sputtering.

The model was applied for processes, nitriding, and annealing, and only in the case of annealing is the adsorption term $\Phi_{0(hkl)}$ excluded from the equations. All other diffusion terms remain the same, and only the values of some parameters and initial conditions are changed. As an initial condition in the case of the simulation of nitriding, the pure ASS, free of nitrogen, was taken. In the case of annealing, as an initial condition, the nitrided ASS with a given nitrogen depth distribution function was taken. To solve the above-presented model equations, the numerical Runge–Kutta methods were used.

It is important to note that the proposed model can be used to describe the nitrogen distribution in ASS during the nitriding and thermal annealing processes at different temperatures until chromium nitride formation, i.e., at temperatures below 450 °C [21–27]. Moreover, for nitrided layers containing the γ_N phase, various types of strain (thermal, compositional, elastic, and plastic) can be considered. However, we only take into account anisotropic compositional strain in our model. Therefore, the incorporation of the compositional, thermal, plastic, and elastic contributions to the strain, induced on austenite lattice due to the formation of the γ_N phase, will be the main task in our future investigations.

3. Results and Discussion

To demonstrate the role played by the various physical phenomena associated with the effects of traps, stress, and solute concentration contained in the continuum model of Equations (4)–(6), we considered a model material of nitrogen solutes in the ASS host where it can be trapped in a chromium atom trap site or detrapped from it. Validation

of the proposed model was performed through the simulation of nitrogen diffusion in single-crystalline ASS AISI 316L during ion beam nitriding at three different crystalline orientations, and subsequent annealing. The experimental results are taken from Ref. [53], where 316L ASS bulk single crystals with (100), (110), and (111) crystalline orientations were nitrided for 60 min at 400 °C and nitrogen ion energy of 1 keV was applied. Further, the nitrided single crystals were subsequently annealed ex situ at 400 °C for 30 min. A detailed description of the sample preparation and experimental conditions is reported in Ref. [53]. It is important to note that the XRD analysis of the virgin, nitrided, and subsequently annealed samples showed the presence of the γ_N phase in the nitrided layer, and no formation of any chromium nitrides was detected (see Figure 1 in Ref. [53]). This fact is important, as nitrogen diffusion during nitriding or annealing can be described by the purposed model. The microstructure of post-nitrided ASS samples was analyzed in our previous work, where the SEM micrographs show very clearly different penetration depths of nitrogen for differently orientated grains (see Figure 3 in Ref. [49]). The material properties of AISI 316L and values of the above-described model parameters used in the numerical simulation and fitting of those experimental results are listed in Table 1.

Table 1. Simulation parameters.

	S_{11}, 1/GPa	S_{12}, 1/GPa	S_{44}, 1/GPa	Zener Ratio
AISI 316L γ phase [54]	9.84×10^{-3}	-3.86×10^{-3}	8.40×10^{-3}	3.26
AISI 316L γ_N phase [55]	4.43×10^{-3}	-1.35×10^{-3}	21.7×10^{-3}	0.53
v_{sp}, cm/s [53]	i_N, s^{-1}	E_A, eV [49]	E_B, eV [49]	Do, cm^2s^{-1}
1.3×10^{-8}	11.8×10^{-4}	1.1	0.23	1.12×10^{-4}
N_0, cm^{-3} [49]	H_t, cm^{-3} [49]	V_N, m^3/mol	R_t, cm [49]	α_N
7.29×10^{22}	1.31×10^{22}	3.9×10^{-5}	0.38×10^{-7}	0.8
β_N, cm/at.% [46]	a_0, cm [46]	$X_{stress(hkl)}$, MPa/at.%		
7.5×10^{-11}	0.36×10^{-7}	X_{stress} values for each of the three considered crystallographic orientations were taken from our previous work [46] (see Figure 2 in [46])		

The experimental and calculated nitrogen depth profiles are presented in Figure 1 for three different crystalline orientations after nitriding (for 60 min at 400 °C) and after isothermal annealing (for 30 min at 400 °C). It is seen that the variations in the nitrogen concentration with depth show unusual concavity (typical for the low-temperature nitriding of ASS), which reflects a forced diffusion regime. Furthermore, there are significant differences in the nitrogen penetration depths and surface nitrogen content for the different crystal orientations, i.e., an increase in surface concentration of nitrogen and nitrogen penetration depth in the order (100) > (110) > (111) for different crystallographic orientations is observed. Such dependences were considered in our previous works [35,38] and explained by the anisotropic nature of the adsorption process due to Gibbs energies for different oriented grains, and internal lattice stress anisotropy, which was determined by taking into account the anisotropy of the Young's modulus for the fcc crystal. In this paper, the experimental observations (Figure 1, points) are quantitatively reproduced (Figure 1, lines) through fitting using the proposed model (Equations (4)–(6)) and by taking into account the anisotropy of crystal lattice stress-induced diffusion under the influence of traps. It is important to note that nitrogen profiles after nitriding were calculated with the same diffusion coefficient for all the different crystallographic orientations of single crystals. However, attempts to obtain good comparisons of the theoretical predictions using experimental data from the nitrogen profiles of annealed samples, with the same diffusion coefficient value as for the nitrided samples (with $D_{nit} = D_{an}$), were unsuccessful. This can be clearly seen in Figure 2, where the nitrogen depth profiles of annealed samples were calculated with different D_{nit}/D_{ann} values. The results presented in Figure 2 indicate that diffusivity during thermal annealing is three times slower than during nitriding. At-

tempts to fit the experimental results with D_{nit}/D_{ann} = 1 and D_{nit}/D_{ann} = 2 result in greater deviation from the experimental points, and only D_{nit}/D_{ann} = 3 exhibits good fitting. Note that good fitting of D_{nit}/D_{ann} = 3 is obtained for all three crystal orientations. The lower diffusivity during post-nitriding thermal annealing than during ion beam nitriding was found in the work [53] using a trapping/detrapping model. In that model, stress-induced diffusion mechanisms were not taken into account, and it was assumed that the diffusion coefficient itself depends on crystallographic orientation. It was found that the diffusion coefficient during the annealing process, compared with the nitriding process, decreases by factors of 4.3, 3.3, and 2.5 for the orientations (001), (011), and (111), respectively. It is most probable that the 1 keV ion bombardment during nitriding has an influence on the enhanced diffusivity [56] during the nitriding process compared with diffusivity in the annealing process, where the surface is not affected and samples are in a rest state. The explanation for this enhanced diffusion during the nitriding process is proposed in Ref. [57], which is based on quasi-particle-enhanced mobility, i.e., the effect of ion bombardment on deep diffusion was explained on the basis of ion irradiation-created quasiparticles that can propagate over long distances in the ASS lattice, interacting with the interstitial atoms and affecting their mobility [57].

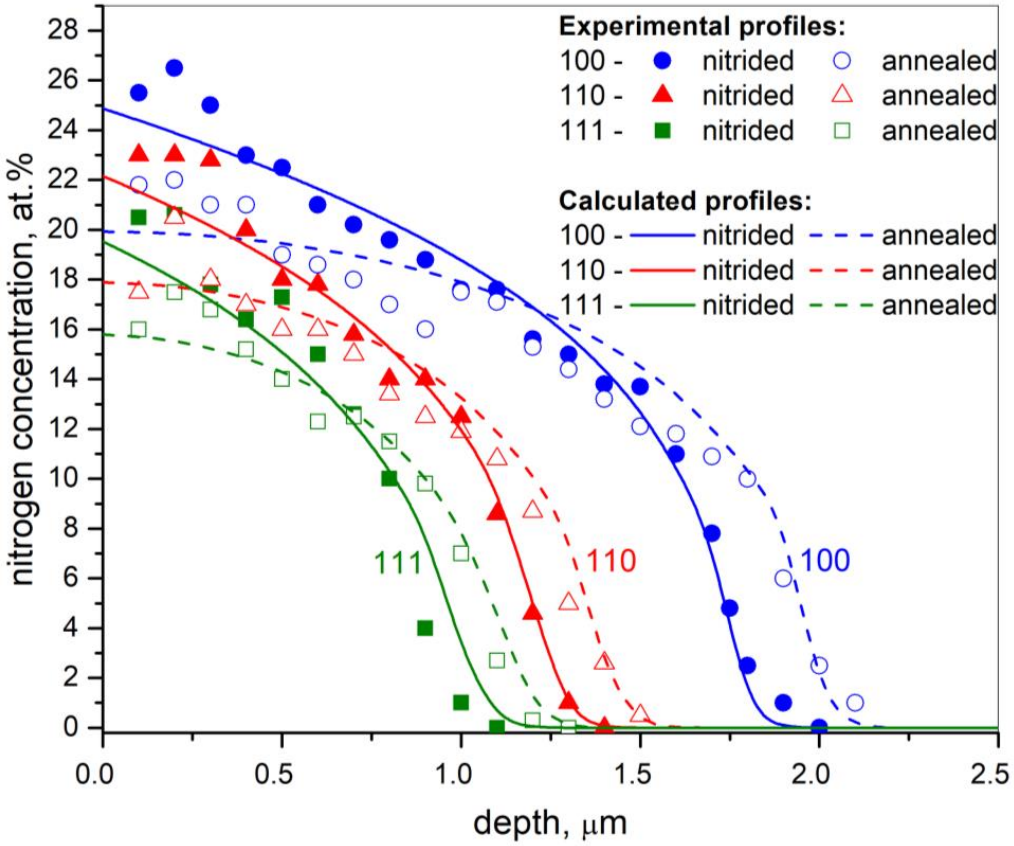


Figure 1. Calculated (lines) and experimental (points, data from [53]) depth profiles of nitrogen in the (100), (110), and (111)-oriented single crystals of ASS. Solid lines: resulting nitrogen profiles after nitriding (for 60 min at 400 °C), dotted lines: resulting nitrogen profiles after isothermal annealing (for 30 min at 400 °C).

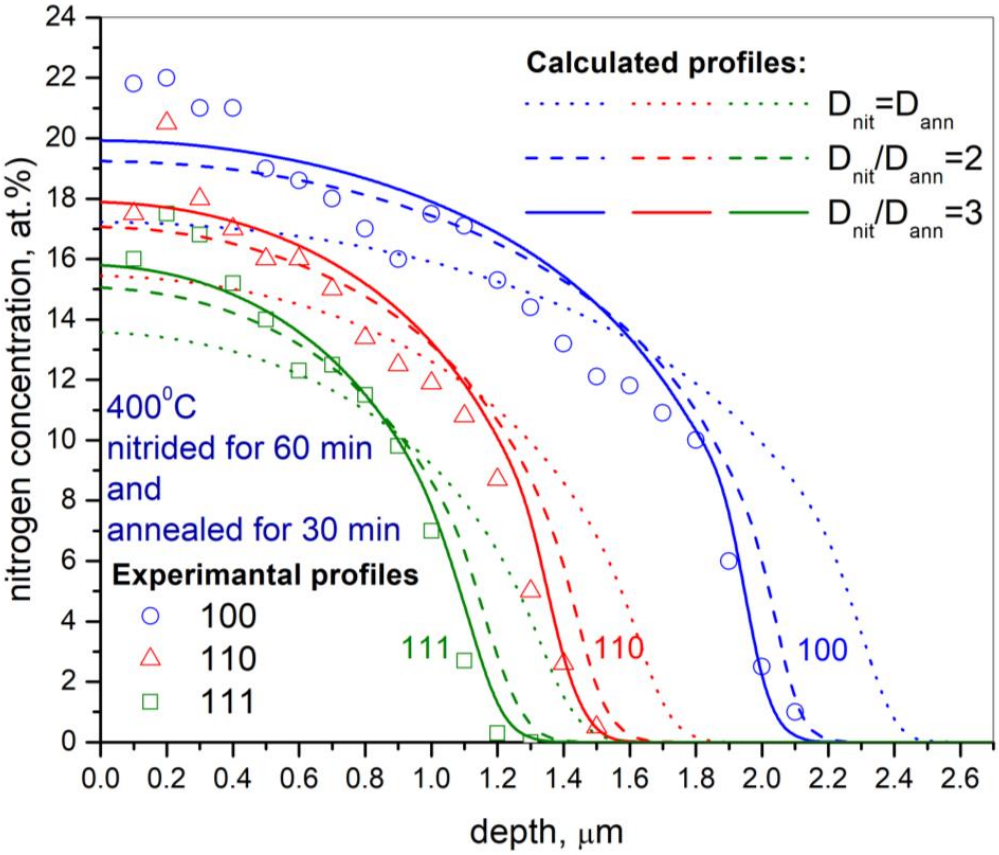


Figure 2. Calculated depth profiles of nitrogen in the (100), (110), and (111)-oriented single crystals of nitrided ASS after isothermal annealing (for 30 min at 400 °C). Experimental results (points) are taken from Ref. [53].

Details of the distribution of nitrogen in the normal lattice N_D and traps N_T after nitriding (for 60 min at 400 °C) and after post-nitriding isothermal annealing (for 30 min at 400 °C) for the cases of D_{nit}/D_{ann} = 1 and D_{nit}/D_{ann} = 3 are shown in Figure 3. By comparing the nitrided and annealed nitrogen profiles, it is seen that the plateau in the annealed profiles is more horizontal. It is seen that the plateau in the total nitrogen depth profile is formed mainly because of nitrogen distribution at the traps sites, which is much higher than for mobile (a diffusive) nitrogen. However, a plateau is observed in the mobile nitrogen profiles after annealing. With the variation in the ratio of D_{nit}/D_{ann}, the balance between mobile nitrogen and nitrogen at the trap sites changes. It can be seen that as the D_{nit}/D_{ann} increases, the penetration depth of nitrogen in both states, diffusing and trapped, decreases. At the same time, the concentration of nitrogen in the surface layers increases. The dependences of surface concentration and nitrogen penetration depth on different crystallographic orientations, as functions of the ratios of D_{nit}/D_{ann}, are presented in Figure 4. Both dependences in Figure 4 are non-linear. As can be seen, nitrogen surface concentration shows an increase with an increase in the ratio of D_{nit}/D_{ann}, while the penetration depth of nitrogen shows the opposite tendency. According to the Arrhenius law, diffusion coefficient increases with temperature, so the results presented in Figure 4 can also be considered to represent the influence of annealing temperature. Diffusion depth is proportional to $\sqrt{Dt}$, i.e., the diffusion coefficient D and diffusion time t influence the diffusion depth in the same way. So, the penetration depths presented in Figure 4 at different diffusion coefficients also can be considered to represent penetration depths for different diffusion times.

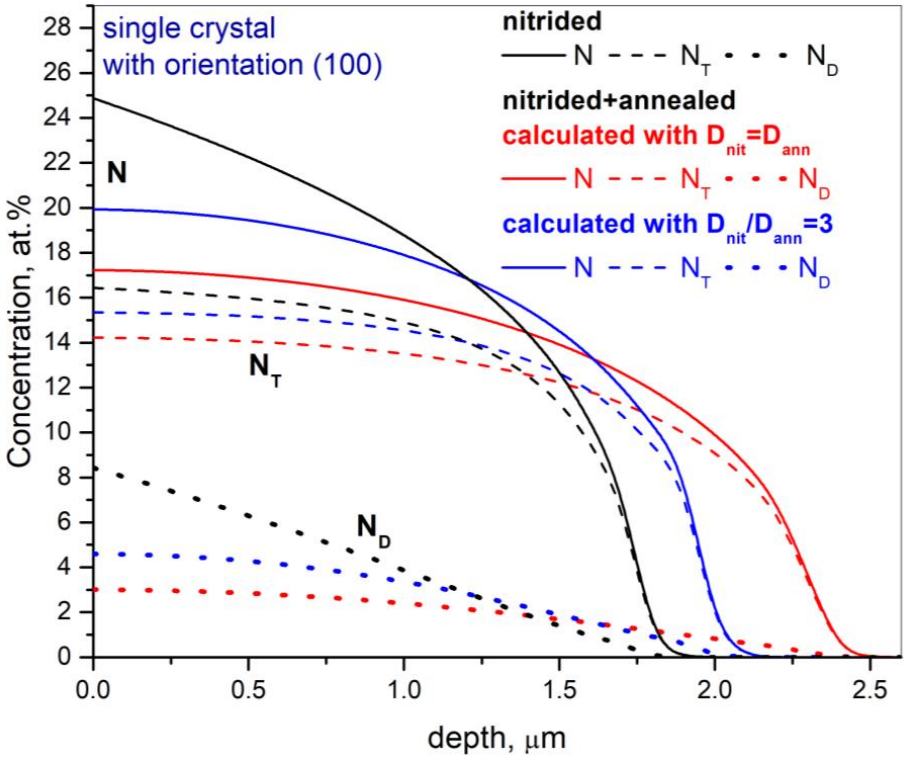


Figure 3. Calculated (with different D_{nit}/D_{ann} ratios) depth profiles of nitrogen in the (100)-oriented single crystal of ASS after nitriding (for 60 min at 400 °C) and after isothermal annealing (for 30 min at 400 °C). N_D—nitrogen in normal lattice, N_T—nitrogen at trap sites, and N—total nitrogen concentration.

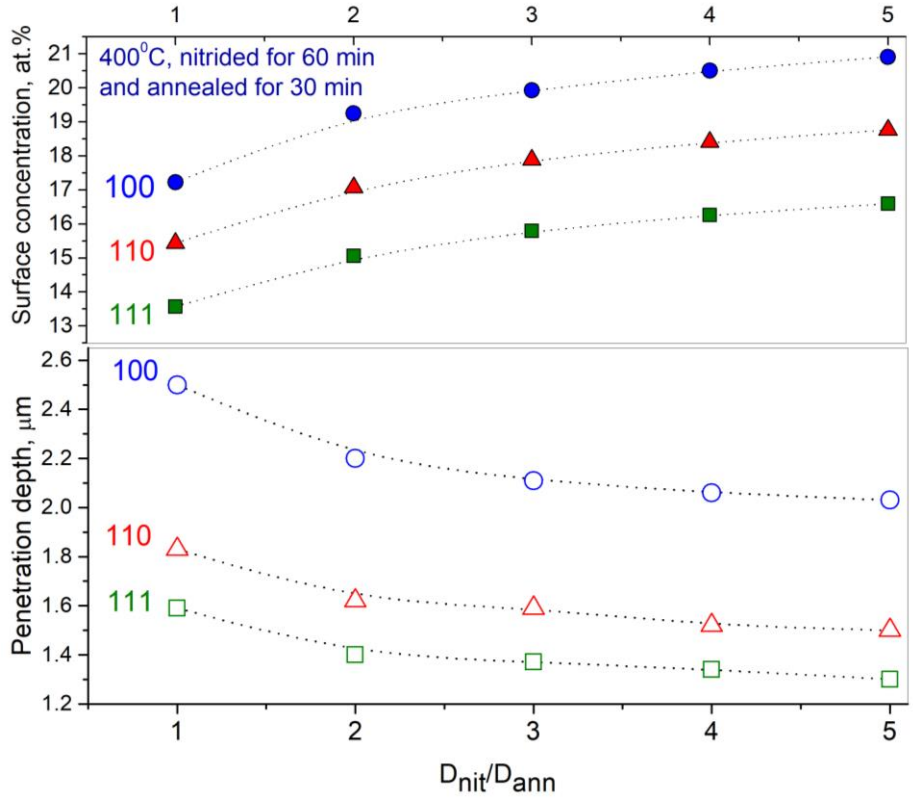


Figure 4. The dependences of nitrogen surface concentration and penetration depth on ratio of D_{nit}/D_{ann} calculated for different crystalline orientations.

A more detailed view of the influence of annealing time on nitrogen distribution with varying depths in nitrided ASS (calculated for (100) crystallographic orientation) is shown in Figure 5. As shown in Figure 5, it is found that longer annealing time results in a thicker nitrided layer and lower nitrogen concentration on the ASS surface. A reduction in surface content and increase in nitride layer thickness indicate that the nitrogen diffuses inward during the annealing process. It is seen that changes in the content of nitrogen at the trap sites N_T in the near-surface layer are not as significant as those in the content of mobile nitrogen N_D. Additionally, quite significant changes in the resulting nitrogen N in the near-surface region occur, mainly due to the mobile nitrogen N_D. However, in deeper regions, the changes in nitrogen content at the traps sites N_T are significant, and this mainly affects the distribution of the resulting nitrogen N, as the amount of mobile nitrogen N_D becomes very low. This phenomenon occurs due to the fact that in the near-surface layers, the number of nitrogen trap sites almost reaches a saturation state, which is determined by parameter H_t in Equation (6) (the value can be seen in Table 1). Detrapping is the process which is determined by parameter E_b in Equation (6) (value in Table 1) and this process is quite slow, so the transition from/to the N_T and N_D near-saturation state which is observed in the near surface layers is quite slow. The situation is different in deeper layers, where N_T is quite far from the saturation state. In this case, the transition of N_D to N_T is fast, which is why in Figure 5, significant changes with annealing time for N_T are observed.

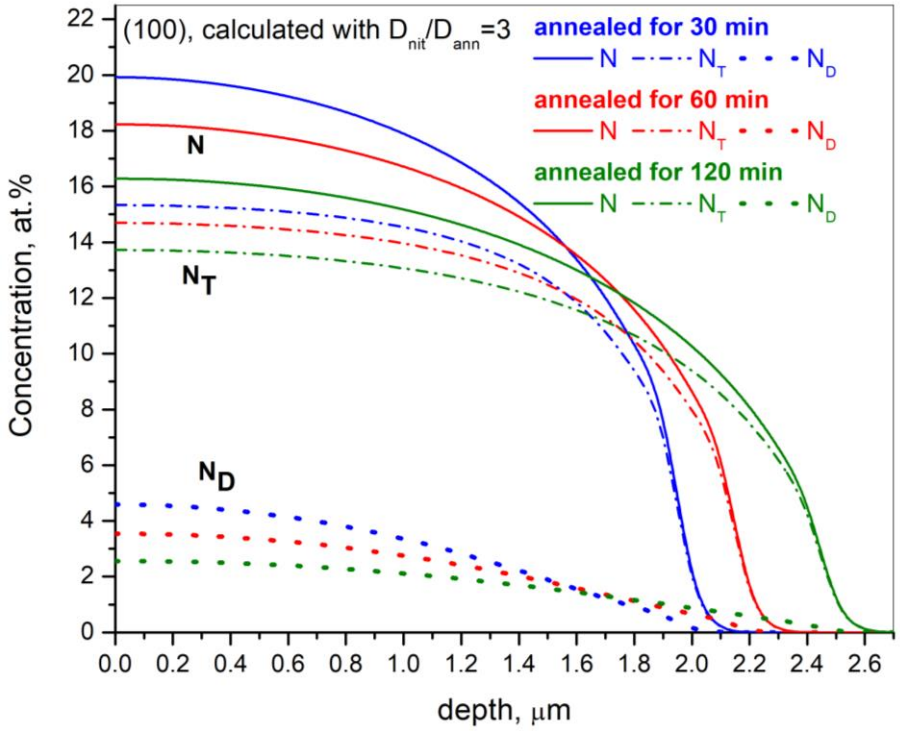


Figure 5. Calculated (with D_{nit}/D_{ann} = 3) depth profiles of nitrogen in the (100)-oriented single crystal of ASS after nitriding (for 60 min at 400 °C) and after isothermal annealing for 30 min, 60 min, and 120 min (at 400 °C). N_D—nitrogen in normal lattice, N_T—nitrogen in trap sites, and N—total nitrogen concentration.

The model presented in this work takes into account stress-assisted diffusion (STRESS) and the trapping/detrapping mechanism (TD). In order to check the influence of each process on the evolution of the nitrogen content in ASS during post-nitriding isothermal annealing, it is necessary to conduct further comparisons. Consequently, Figure 6 presents the calculated results, together with experimental points [53], for different cases during isothermal annealing, including: (1) both processes (trapping/detrapping and stress-assisted diffusion (curve for TD + STRESS)), (2) only the stress-assisted diffusion process (curve

for no-TD), and (3) only the trapping/detrapping mechanism (curves for no-STRESS with different D_{nit}/D_{ann} values). Firstly, the presented results show that the exclusion of the trapping/detrapping process is an incorrect choice as the calculated profile does not fit the experimental points at all (see curve for no-TD). The profiles calculated with exclusion of the stress-induced diffusion (see curves for no STRESS) process exhibit much better fitting. Furthermore, attempts were made to fit the experimental points using the model without the stress-induced diffusion process but with different diffusion coefficients (different ratio of $D_{ni}t/D_{ann}$, where $D_{nit} = const.$). As can be seen in Figure 6, with an increase in D_{ann} (i.e., a decrease in the ratio of D_{nit}/D_{ann}) the nitrogen profiles change so that nitrogen concentration on the steel surface decreases and penetration depth increases. From the point of view of modeling, it would be possible to determine the optimal value of the ratio of D_{nit}/D_{ann} and obtain a good comparison of the theoretical predictions with experimental data. However, it is very important to note that the diffusion behavior of nitrogen in steel is affected by not only the interstitial solute concentration but also the stress induced by nitrogen atoms expanding the lattice of the alloy. The existence of lattice stress during the nitriding of stainless steels and the anisotropic nature of the stress were proved experimentally [8,36,37,58,59] and via modeling in our previous work [35,38] and that of other authors [41–43,58–60]. So, it is necessary to evaluate this process during calculations and for best fitting to be determined when both processes are included (Figure 6, curve for TD + STRESS), i.e., stress-induced diffusion and trapping/detrapping are the processes that actually occur during the nitriding of ASS.

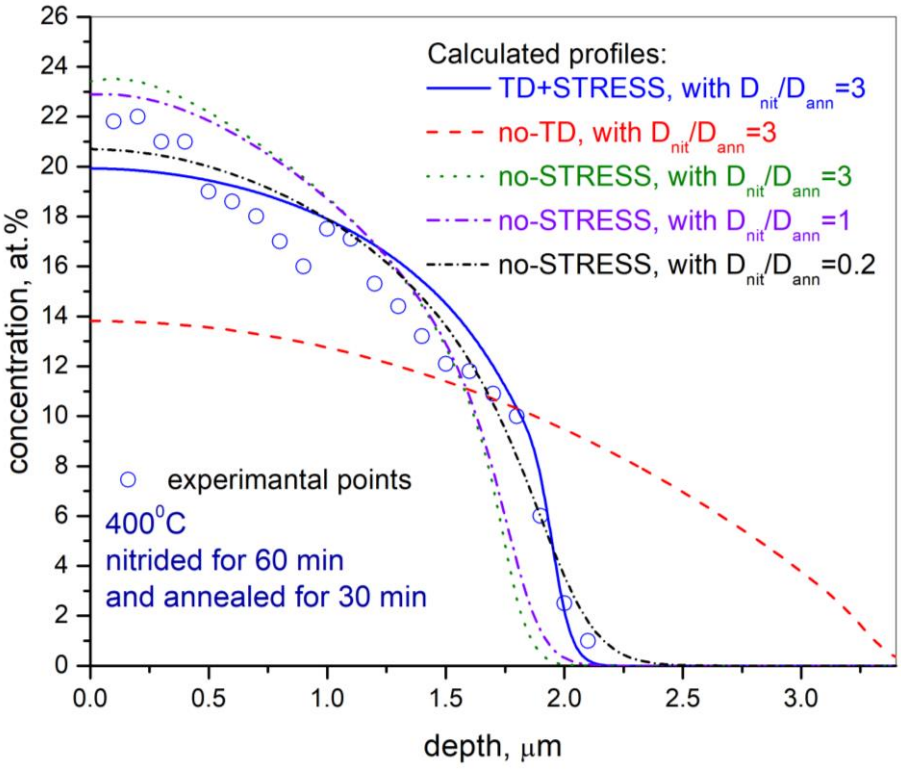


Figure 6. Calculated depth profiles of total nitrogen in the (100)-oriented single crystal of ASS for three cases, including: (1) both processes (trapping/detrapping (TD) and stress-induced diffusion (STRESS)) (curve for TD + STRESS), (2) only the process of STRESS (curve for no-TD), and (3) only the TD model (curves for no-STRESS with different D_{nit}/D_{ann} ratios). Experimental results (points) are taken from Ref. [53].

4. Conclusions

Nitrogen diffusion in single-crystalline austenitic stainless steel during modified layer formation and thermal annealing was analyzed using the presented kinetic model. The main conclusions are as follows:

1. During the nitriding and post-nitriding annealing of austenitic stainless steels, the same diffusion mechanisms take place: trapping/detrapping and lattice stress-induced diffusion.
2. The anisotropic nature of mass transport processes, i.e., dependence on crystallographic lattice orientation, is observed during both processes of nitriding and post-nitriding isothermal annealing.
3. The trapping/detrapping process has a main influence on the specific distribution depth profile of nitrogen in post-nitrided and post-annealed ASS. However, lattice stress-induced diffusion cannot be excluded.
4. Nitrogen diffusivity during post-nitriding thermal annealing is significantly lower than during nitriding. The diffusion coefficient during the annealing process, compared with the nitriding process, decreases by factors of 4.3, 3.3, and 2.5 for the orientations (001), (011), and (111), respectively.

It follows from above conclusions that the application of the thermal annealing procedure for phase stabilization and stress relaxation of post-nitrided ASS samples leads to significant changes in nitrogen distribution, as well as influencing the physical and mechanical properties of ASS.

Author Contributions: Conceptualization, A.G. and T.M.; methodology, A.G. and T.M.; software, T.M. and P.A.; validation, A.G., T.M. and P.A.; formal analysis, A.G., T.M. and P.A.; investigation, A.G. and T.M.; resources, A.G. and T.M.; data curation, A.G. and T.M.; writing—original draft preparation, A.G., T.M. and P.A.; writing—review and editing, A.G. and T.M.; visualization, T.M.; supervision, A.G. All authors have read and agreed to the published version of the manuscript.

Funding: This research received no external funding.

Institutional Review Board Statement: Not applicable.

Informed Consent Statement: Not applicable.

Data Availability Statement: Not applicable.

Conflicts of Interest: The authors declare no conflict of interest.

References

1. Menthe, E.; Rie, K.T.; Schultze, J.W.; Simson, S. Structure and properties of plasma-nitrided stainless steel. *Surf. Coat. Technol.* **1995**, *74–75*, 412. [CrossRef]
2. De Las Heras, E.; Ybarra, G.; Lamas, D.; Cabo, A.; Dalibon, E.L.; Brühl, S.P. Plasma nitriding of 316L stainless steel in two different N2-H2 atmospheres—influence on microstructure and corrosion resistance. *Surf. Coat. Technol.* **2017**, *313*, 47–54. [CrossRef]
3. Menthe, E.; Rie, K.T. Further investigation of the structure and properties of austenitic stainless steel after plasma nitriding. *Surf. Coat. Technol.* **1999**, *116–119*, 199–204. [CrossRef]
4. Mingolo, N.; Tschiptschin, A.P.; Pinedo, C.E. On the formation of expanded austenite during plasma nitriding of an AISI 316L austenitic stainless steel. *Surf. Coat. Technol.* **2006**, *201*, 4215–4218. [CrossRef]
5. Keddam, M.; Marcos, G.; Thiriet, T.; Czerwiec, T.; Michel, H. Microstructural characterization of the expanded austenite formed on the plasma nitrided AISI 316 L steel. *Mater. Tech.* **2013**, *101*, 204. [CrossRef]
6. Baldwin, M.J.; Fewell, M.P.; Haydon, S.C.; Kumar, S.; Collins, G.A.; Short, K.T.; Tendys, J. Rf-plasma nitriding of stainless steel. *Surf. Coat. Technol.* **1998**, *98*, 1187. [CrossRef]
7. Fewell, M.P.; Mitchell, D.R.G.; Priest, J.M.; Short, K.T.; Collins, G.A. The nature of expanded austenite. *Surf. Coat. Technol.* **2000**, *131*, 300–306. [CrossRef]
8. Christiansen, T.L.; Hummelshøj, T.S.; Somers, M.A.J. Expanded austenite, crystallography and residual stress. *Surf. Eng.* **2010**, *26*, 242–247. [CrossRef]
9. Picard, S.; Memet, J.B.; Sabot, R.; Grosseau-Poussard, J.L.; Rivière, J.P.; Meilland, R. Corrosion behaviour, microhardness and surface characterisation of low energy, high current ion implanted austenitic stainless steel. *Mater. Sci. Eng. A* **2001**, *303*, 163–172. [CrossRef]

10. Baranowska, J. Characteristic of the nitrided layers on the stainless steel at low temperature. *Surf. Coat. Technol.* **2004**, *180–181*, 145–149. [CrossRef]
11. Williamson, D.L.; Davis, J.A.; Wilbur, P.J. Effect of austenitic stainless steel composition on low-energy, high-flux, nitrogen ion beam processing. *Surf. Coat. Technol.* **1998**, *103–104*, 178. [CrossRef]
12. He, H.; Czerwiec, T.; Dong, C.; Michel, H. Effect of grain orientation on the nitriding rate of a nickel base alloy studied by electron backscatter diffraction. *Surf. Coat. Technol.* **2003**, *163*, 331. [CrossRef]
13. Czerwiec, T.; Renevier, N.; Michel, H. Low-temperature plasma-assisted nitriding. *Surf. Coat. Technol.* **2000**, *131*, 267. [CrossRef]
14. Dahm, K.L.; Dearnley, P.A. On the nature, properties and wear response of S-phase (nitrogen alloyed stainless steel) coatings on AISI 316L. *Proc. Inst. Mech. Eng.* **2000**, *214*, 181–198. [CrossRef]
15. Saker, A.; He, H.; Czerwiec, T.; Li, X.; Huu, L.T.; Dong, C.; Michel, H.; Frantz, C. Reactive magnetron sputtering of Inconel 690 by Ar–N2 plasma. *Thin Solid Films* **2008**, *516*, 1029–1036. [CrossRef]
16. Terwagne, G.; Colaux, J.; Mitchell, D.R.; Short, K.T. Temperature effect of nitride stainless steel coatings deposited by reactive DC-magnetron sputtering. *Thin Solid Films* **2004**, *469–470*, 167–172. [CrossRef]
17. Baranowska, J.; Fryska, S.; Przekop, J.; Suszko, T. The properties of hard coating composed of S-phase obtained by PVD method. *Adv. Manuf. Sci. Technol.* **2009**, *33*, 59–69.
18. Fryska, S.; Baranowska, J. Microstructure of reactive magnetron sputtered S-phase coatings with a diffusion sub-layer. *Vacuum* **2017**, *142*, 72–80. [CrossRef]
19. Kappaganthu, S.R.; Sun, Y. Influence of sputter deposition conditions on phase evolution in nitrogen-doped stainless steel films. *Surf. Coat. Technol.* **2005**, *198*, 59. [CrossRef]
20. Baranowska, J.; Fryska, S.; Suszko, T. The influence of temperature on S-phase coatings deposition by reactive magnetron sputtering. *Vacuum* **2013**, *90*, 160–164. [CrossRef]
21. Czerwiec, T.; Andrieux, A.; Marcos, G.; Michel, H.; Bauer, P. Is "expanded austenite" really a solid solution? Mossbauer observation of an annealed AISI 316L nitrided sample. *J. Alloy. Compd.* **2019**, *811*, 151972. [CrossRef]
22. Jirásková, Y.; Blawert, C.; Schneeweiss, O. Thermal Stability of Stainless Steel Surfaces Nitrided by Plasma Immersion Ion Implantation. *Phys. Status Solidi* **1999**, *175*, 537–548. [CrossRef]
23. Borgioli, F. The "Expanded" Phases in the Low-Temperature Treated Stainless Steels: A Review. *Metals* **2022**, *12*, 331. [CrossRef]
24. Wang, J.; Li, Z.; Wang, D.; Qiu, S.; Ernst, F. Thermal stability of low-temperature-carburized austenitic stainless steel. *Acta Mater.* **2017**, *128*, 235–240. [CrossRef]
25. Molleja, G.; Milanese, M.; Piccoli, M.; Moroso, R.; Niedbalski, J.; Nosei, L.; Feugeas, J. Stability of expanded austenite, generated by ion carburizing and ion nitriding of AISI 316L SS, under high temperature and high energy pulsed ion beam irradiation. *Surf. Coat. Technol.* **2013**, *218*, 142–151. [CrossRef]
26. Tschiptschin, A.P.; Nishikawa, A.S.; Varela, L.B.; Pinedo, C.E. Thermal stability of expanded austenite formed on a DC plasma nitrided 316L austenitic stainless steel. *Thin Solid Films* **2017**, *644*, 156–165. [CrossRef]
27. Djellal, R.; Saker, A.; Bouzabata, B.; Mekki, D.E. Thermal stability and phase decomposition of nitrided layers on 316L and 310 austenitic stainless steels. *Surf. Coat. Technol.* **2017**, *325*, 533–538. [CrossRef]
28. Wu, D.; Kahn, H.; Dalton, J.C.; Michal, G.M.; Ernst, F.; Heuer, A.H. Orientation dependence of nitrogen supersaturation in austenitic stainless steel during low-temperature gas-phase nitriding. *Acta Mater.* **2014**, *79*, 339. [CrossRef]
29. Menéndez, E.; Templier, C.; Garcia-Ramirez, P.; Santiso, J.; Vantomme, A.; Temst, K.; Nogués, J. Magnetic properties of single crystalline expanded austenite obtained by plasma nitriding of austenitic stainless steel single crystals. *ACS Appl. Mater. Interfaces* **2013**, *5*, 10118–10126. [CrossRef] [PubMed]
30. Fewell, M.P.; Priest, J.M. High-order diffractometry of expanded austenite using synchrotron radiation. *Surf. Coat. Technol.* **2008**, *202*, 802–1815. [CrossRef]
31. Borgioli, F. From austenitic stainless steel to expanded austenite-S phase: Formation, characteristics and properties of an elusive metastable phase. *Metals* **2020**, *10*, 187. [CrossRef]
32. Martinavičius, A.; Abrasonis, G.; Möller, W. Influence of crystal orientation and ion bombardment on the nitrogen diffusivity in single-crystalline austenitic stainless steel. *J. Appl. Phys.* **2011**, *110*, 075907. [CrossRef]
33. Kahn, H.; Michal, G.M.; Ernst, F.; Heuer, A.H. Poisson effects on X-ray diffraction patterns in low-temperature-carburized austenitic stainless steel. *Metall. Mater. Trans. A* **2009**, *40*, 1799–1804. [CrossRef]
34. He, H.; Zou, J.X.; Dong, C.; Czerwiec, T.; Michel, H. Stress induced anisotropic diffusion during plasma-assisted nitriding of a Ni-based alloy. *Mater. Sci. Forum* **2005**, *475*, 3669–3672. [CrossRef]
35. Moskalioviene, T.; Galdikas, A. Crystallographic Orientation Dependence of Nitrogen Mass Transport in Austenitic Stainless Steel. *Metals* **2020**, *10*, 615. [CrossRef]
36. Somers, M.A.J.; Kücükyildiz, Ö.C.; Ormstrup, C.A.; Alimadadi, H.; Hattel, J.H.; Christiansen, T.L.; Winther, G. Residual stress in expanded austenite on stainless steel; origin, measurement, and prediction. *Mater. Perform. Charact.* **2018**, *7*, 693–716. [CrossRef]
37. Mändl, S.; Rauschenbach, B. Anisotropic strain in nitrided austenitic stainless steel. *J. Appl. Phys.* **2000**, *88*, 3323–3329. [CrossRef]
38. Moskalioviene, T.; Galdikas, A. Kinetic model of anisotropic stress assisted diffusion of nitrogen in nitrided austenitic stainless steel. *Surf. Coat. Technol.* **2019**, *366*, 277–285. [CrossRef]
39. Galdikas, A.; Moskalioviene, T. Modeling of stress induced nitrogen diffusion in nitrided stainless steel. *Surf. Coat. Technol.* **2011**, *205*, 3742–3746. [CrossRef]

40. Moskalioviene, T.; Galdikas, A. Stress induced and concentration dependent diffusion of nitrogen in plasma nitrided austenitic stainless steel. *Vacuum* **2012**, *86*, 1552–1557. [CrossRef]
41. Jespersen, F.N.; Hattel, J.H.; Somers, M.A.J. Modelling the evolution of composition-and stress-depth profiles in austenitic stainless steels during low-temperature nitriding. *Model. Simul. Mat. Sci. Eng.* **2016**, *24*, 025003. [CrossRef]
42. Kücükyildiz, Ö.C.; Grumsen, F.B.; Christiansen, T.L.; Winther, G.; Somers, M.A.J. Anisotropy effects on gaseous nitriding of austenitic stainless steel single crystals. *Acta Mater.* **2020**, *194*, 168–177. [CrossRef]
43. Christiansen, T.L.; Somers, M.A.J. The Influence of Stress on Interstitial Diffusion—Carbon Diffusion Data in Austenite Revisited. *Defect Diffus. Forum* **2010**, *297–301*, 1408–1413. [CrossRef]
44. Parascandola, S.; Moller, W.; Williamson, D.L. The nitrogen transport in austenitic stainless steel at moderate temperatures. *Appl. Phys. Lett.* **2000**, *76*, 2194–2196. [CrossRef]
45. Christiansen, T.L.; Drouet, M.; Martinavičius, A.; Somers, M.A.J. Isotope exchange investigation of nitrogen redistribution in expanded austenite. *Scr. Mater.* **2013**, *69*, 582–585. [CrossRef]
46. Galdikas, A.; Moskalioviene, T. The Anisotropic Stress-Induced Diffusion and Trapping of Nitrogen in Austenitic Stainless Steel during Nitriding. *Metals* **2020**, *10*, 1319. [CrossRef]
47. Mändl, S.; Scholze, F.; Neumann, H.; Rauschenbach, B. Nitrogen diffusivity in expanded austenite. *Surf. Coat. Technol.* **2003**, *174–175*, 1191–1195. [CrossRef]
48. Oriani, R. The diffusion and trapping of hydrogen in steel. *Acta Metall.* **1970**, *18*, 147–157. [CrossRef]
49. Moskalioviene, T.; Galdikas, A.; Riviere, J.P.; Pichon, L. Modeling of nitrogen penetration in polycrystalline AISI 316L austenitic stainless steel during plasma nitriding. *Surf. Coat. Technol.* **2011**, *205*, 3301–3306. [CrossRef]
50. Möller, W.; Parascandola, S.; Telbizova, T.; Günzel, R.; Richter, E. Surface processes and diffusion mechanisms of ion nitriding of stainless steel and aluminium. *Surf. Coat. Technol.* **2001**, *136*, 73–79. [CrossRef]
51. Zhang, L.; Barrett, R.; Cloetens, P.; Detlefs, C.; Rio, M.S. Anisotropic elasticity of silicon and its application to the modelling of X-ray optics. *J. Synchrotron. Radiat.* **2014**, *21*, 507–517. [CrossRef] [PubMed]
52. Zener, C. Contributions to the Theory of Beta-Phase Alloys. *Phys. Rev.* **1947**, *71*, 846–851. [CrossRef]
53. Martinavičius, A.; Abrasonis, G.; Möller, W.; Templier, C.; Rivière, J.P.; Declémy, A.; Chumlyakov, Y. Anisotropic ion-enhanced diffusion during ion nitriding of single crystalline austenitic stainless steel. *J. Appl. Phys.* **2009**, *105*, 93502. [CrossRef]
54. Juul, N.Y.; Oddershede, J.; Beaudoin, A.; Chatterjee, K.; Koker, M.K.A.; Dale, D.; Shade, P.; Winther, G. Measured resolved shear stresses and Bishop-Hill stress states in individual grains of austenitic stainless steel. *Acta Mater.* **2017**, *141*, 388–404. [CrossRef]
55. Gressmann, T.; Wohlschlogel, M.; Shang, S.; Welzel, U.; Leineweber, A.; Mittemeijer, E.J.; Liu, Z.K. Elastic anisotropy of γ′-Fe4N and elastic grain interaction in γ′-Fe4N1−y layers on α-Fe: First-principles calculations and diffraction stress measurements. *Acta Mater.* **2007**, *55*, 5833–5843. [CrossRef]
56. Galdikas, A.; Pranevičius, L. Surface composition changes of ternary alloys in the non-steady state regime of preferential sputtering. *Nucl. Instruments Methods Phys. Res. Sect. B Beam Interact. Mater. Atoms* **2000**, *164*, 868–872. [CrossRef]
57. Abrasonis, G.; Möller, W.; Ma, X.X. Anomalous Ion Accelerated Bulk Diffusion of Interstitial Nitrogen. *Phys. Rev. Lett.* **2006**, *96*, 065901. [CrossRef]
58. Akhlaghi, M.; Jung, M.; Meka, S.R.; Fonović, M.; Leineweber, A.; Mittemeijer, E.J. Dependence of the nitriding rate of ferritic and austenitic substrates on the crystallographic orientation of surface grains; gaseous nitriding of Fe-Cr and Ni-Ti alloys. *Philos. Mag.* **2015**, *95*, 4143–4160. [CrossRef]
59. Christiansen, T.; Dahl, K.V.; Somers, M.A.J. Nitrogen diffusion and nitrogen depth profiles in expanded austenite: Experimental assessment, numerical simulation and role of stress. *Mater. Sci. Technol.* **2008**, *24*, 159–167. [CrossRef]
60. Kücükyildiz, Ö.C.; Sonne, M.R.; Thorborg, J.; Somers, M.A.J.; Hattel, J.H. Thermo-chemical-mechanical simulation of low temperature nitriding of austenitic stainless steel; inverse modelling of surface reaction rates. *Surf. Coat. Technol.* **2020**, *381*, 125145. [CrossRef]

Disclaimer/Publisher's Note: The statements, opinions and data contained in all publications are solely those of the individual author(s) and contributor(s) and not of MDPI and/or the editor(s). MDPI and/or the editor(s) disclaim responsibility for any injury to people or property resulting from any ideas, methods, instructions or products referred to in the content.